Journal of The Electrochemical Society, 2022 **169** 113504
1945-7111/2022/169(11)/113504/12/$40.00 © 2022 The Electrochemical Society ("ECS"). Published on behalf of ECS by IOP Publishing Limited

Highly Efficient Inner Surface Polishing of Fe-Cr-Ni Alloy Cylinder via Isotropically Tuned Electrochemical Etching

Muhammad Ajmal Khan,[1,2] Zejin Zhan,[2] Rong Yi,[2] Jianwei Ji,[2] Linfeng Zhang,[2] Xinquan Zhang,[1,z] and Hui Deng[2,z]

[1]*School of Mechanical Engineering, Shanghai Jiao Tong University, Shanghai, 200240, People's Republic of China*
[2]*Department of Mechanical and Energy Engineering, Southern University of Science and Technology, Shenzhen, Guangdong 518055, People's Republic of China*

In this study, the inner surface of a Fe-Cr-Ni alloy cylinder produced through extrusion is processed by electrochemical isotropic etching polishing (IEP). The electric field simulation predicted a high current density at protrudes, pertinent for passivation layer breakdown and proficient dissolution. Initially, the effect of cathode diameter and current density was investigated on planarization and current efficiencies, material removal rate (MRR), and etching behavior of IEP of grinded Fe-Cr-Ni alloy. IEP of the as-extruded inner surface realized a 94% improvement in the Sa roughness (from 5.33 μm to 0.34 μm), while the initial surface morphology and instantaneously breaking metal lumps seriously influenced the final Sa roughness and polishing duration. Furthermore, the as-extruded and grinded Fe-Cr-Ni alloy substrates were polished simultaneously, whereupon the IEP of the latter produced a mirror-like, highly uniform, and mechanically superior surface with 37% higher planarization efficiency and 19% greater wall thickness. However, due to falling off metal lumps, the IEP of the as-extruded substrate registered higher current efficiency (~38%) than the grinded substrate (~30%). IEP realizing a rapid improvement in the line profile and Ra roughness of the grinded Fe-Cr-Ni alloy shows that IEP can efficiently improve the performance of functional inner surfaces to application grade.
 [DOI: 10.1149/1945-7111/aca361]

Manuscript submitted August 21, 2022; revised manuscript received September 24, 2022. Published November 25, 2022.

Aerospace and automotive are the two largest sectors capitalizing on metals and alloys. Various components such as flanges, valves, and connecting pipes made of metals and alloys are crucial parts of the large machinery manufactured in aero-to-auto industries and atomic energy, and Fe-Cr-Ni alloys have widely served the purpose due to high strength, excellent corrosion resistance, weldability, and the heat resistant nature.[1,2] The surfaces of these parts, particularly the functional inner channels, should be exceedingly smooth to operate machinery properly. Nevertheless, the inner surfaces of the as-build components, manufactured either mechanically or additively, suffer from high surface roughness. Extrusion is one of the most widely used techniques to produce functional metallic cylinders. The inner surface morphologies of the as-extruded cylinders are extremely deteriorated by the surface condition of the die,[3] extrusion parameters such as load, sliding distance, temperature, and pressure, which significantly reinforce plastic deformation[4] and worsen the surface roughness.[5] The high surface roughness of the as-extruded inner surfaces is troublesome for liquid or gas flow and makes them more sensitive to obstruction, corrosion, and mechanical failure. Ramachandran et al.[6] discussed that imparting radii with high-quality surfaces improves gas flow and reduces boundary layer turbulence. Therefore, the inner surface finishing is compulsory. Recently several inner surface polishing approaches have been proposed, such as abrasive and hydrodynamic abrasive finishing, multi-jet polishing, chemo-polishing, electrochemical polishing (ECP), and so on. Hashimoto et al.[7] discussed that mechanical or abrasive polishing is a conventional metal finishing technique that cannot achieve an atomic-scale surface finish due to its scratch-inducing nature. Zhao et al.[8] designed a soft abrasive rotating jet and achieved a 79.8% improvement in the inner surface roughness. Under optimized conditions, the inner surface roughness was reduced from 1.05 μm to 0.212 μm after 90 min of polishing, showing that planarization efficiency was low and the final roughness was still very high. Similarly, hydrodynamic cavitation abrasive finishing (HCAF) achieved more than 90% improvement in the surface roughness with an acceptable thickness loss (45 μm) on the additively manufactured (AM) AlSi10Mg inner surface, but removing attached powder particles took 150 min long time.[9] A multi-jet polishing approach reduced the inner surface Ra roughness to ~20 nm, but a few tens of nanometer roughness was far below the initial roughness of the surfaces manufactured by additive or mechanical methods.[10] High energy beam polishing can significantly enhance the metal surface quality. For example, a two-step laser beam polishing achieved 72% improvement in the Ti6Al4V surfaces where the first step used the effect of the thermocapillary flow to remove high surface roughness, while the residual process features were removed in the second step.[11] Okada et al.[12] used a large area electron beam to polish stainless steel orthopedic surgical tools without requiring beam focusing. Still, the surface oxidation and heat-affected zones (HAZ) generated by energy beam polishing inevitably degraded the mechanical properties and microstructures of the metal surface.[13] In addition, controlling the local irregular flow of melt pools due to gravity, especially for curved surfaces, is very problematic. In general, internal surface finishing is challenging by using mechanical or laser polishing due to the rigidity of these techniques and nearly impossible access to invisible areas. In comparison, chemical and electrochemical methods are proficient at polishing internal surfaces because the working electrolytes can adaptably access impenetrable regions. Tyagi et al.[14] conducted chemical and electrochemical polishing of the AM 316 steel and reported that ECP is more efficient but limited by the counter electrode accessibility when polishing inner surfaces. ECP of the AM Inconel 625 achieved 80% improvement in the inner surface roughness, but a significant difference in the final surface roughness of flat regions (3.02 μm) and round sides (5.82 μm) was observed, possibly due to variation in the passivation layer thickness with substrate geometry.[15] Similarly, the ECP of an additively manufactured nickel-titanium shape memory alloy also found a strong disparity in the inner surface roughness with variation in the channel orientation.[16] Thus, ECP is an extensively used abrasion-free metal finishing technique that depends on the leveling effect of the viscous layer. In ECP, the viscous layer facing the substrate adapts to the surface features while remaining flat on the electrolyte side. As a result, the viscous layer remains comparatively thin at the protruding region, has low electrical resistance, and experiences higher current density. As a consequence of ECP, protrusions are dissolved, and a smooth glossy surface is evolved.[17] A range of metals and alloys, as discussed above, has been successfully polished using ECP. Another novel electrochemical-based isotropic etching polishing (IEP) technique was recently introduced as a generic method of atomically polishing metals and alloys.[18] The IEP was further explored and

[z]E-mail: zhangxinquan@sjtu.edu.cn; dengh@sustech.edu.cn

successfully employed to achieve nanometer and sub-nanometer surface roughness of additively and mechanically manufactured Inconel 718 alloys,[19,20] demonstrating its viability as a futuristic atomic and close-to-atomic scale manufacturing (ACSM) technique.[21] IEP is realized by merging isotropic etching holes formed after breaking the viscous layer at protruding sites. The breakdown of the viscous layer helps in overcoming its electrical resistance making IEP more efficient in metal surface polishing. In addition, the formation and merging of isotropic etching holes for surface smoothening make the polishing mechanism of IEP entirely different from the ECP.

Regardless of numerous studies on the inner surface finishing through electrochemical techniques: (i) the inner surface finishing of the as-extruded, (ii) large area substrate, and (iii) a comprehensive approach to transforming a highly rough inner surface into a mirror-like surface while investigating the mechanism and different aspects of electrochemical polishing have not been discussed. In this work, the isotropically tuned electrochemical etching polishing of the heat resistant Fe-Cr-Ni alloy cylinder is realized to enhance the internal surface roughness. Changes in the inner surface morphologies, roughness, and profiles of the axially sectioned Fe-Cr-Ni cylindrical substrates before and after polishing were measured in addition to the current efficiency, required voltage, and material removal rate (MRR) to support planarization efficiency and polishing mechanism of IEP. The IEP realized a significant improvement in the inner surface roughness of the heat resistant Fe-Cr-Ni alloy, demonstrating it as an efficient polishing technique.

Material and Experiments

Electrochemical isotropic etching polishing of Fe-Cr-Ni alloy.—The mechanism and scope of IEP and the experimental setup of electrochemical isotropic polishing of heat resistant Fe-Cr-Ni alloy are schematized in Fig. 1. The IEP is contingent upon passive layer breakdown and the formation of isotropic etching holes and their merging. As shown in Fig. 1a, the localized isotropic etching initiates through small holes in the passivation layer due to the application of an external electric field. As IEP progresses, the metals dissolve, and etching holes are generated under the passivation layer. Since the passivation layer limits the diffusion of metallic ions in the electrolyte, they concentrate in etching holes, and the dissolution becomes mass controlled. Consequently, impurities induced preferential etching is suppressed, and isotropic etching holes with low surface roughness are formed. These isotropic etching holes merge and form a smooth surface, while the passivation layer drops due to reducing contact area. Recent investigations on the IEP of Titanium[18] and Inconel 718, both 3D printed[19] and as-casted,[20] have intensively verified this mechanism. In addition, the electrolyte concentration and temperature have been found to influence the nature of electrochemical etching. In these investigations, IEP efficiently improved the corrosion resistance and realized nano-to-sub-nanometer surface roughness of 3D printed and as-casted surfaces with their geometries varying from flat to complex, as shown in Fig. 1b. Polishing flat and complex geometries with equally high efficiency has proven IEP an established metal polishing technique. However, inner surface finishing is rather challenging due to inaccessible inner features attributed to narrow sizes, closed geometries, and high roughness caused by poor manufacturing, such as rough extrusion.

In this study, the IEP of the inner surface of a Fe-Cr-Ni alloy cylinder with internal diameter $d_{in} = 12$ mm and thickness $T = 2$ mm was realized in an electrolyte comprised of 20 ml H_2SO_4 and 100 ml CH_3OH, subsequently written as 20 ml H_2SO_4 electrolyte. The commercial-grade H_2SO_4−97% in the IEP electrolyte can etch the metal surface, while CH_3OH-99.5% can destabilize the passivation film and form metal complexes. The heat resistant Fe-Cr-Ni alloy cylinder substrates were initially produced by extrusion. Later, the cylindrical substrates were vertically sectioned into equal halves for characterization before and after processing. A Teflon holder was designed to grip the cross-sectioned halves in a cylindrical shape and align the stainless-steel rod cathodes in the middle to maintain a uniform electric field throughout the inner surface of the anode. The experimental setup, steel cathodes with different diameters, Teflon holder, and electrolyte chemistry are shown in Figs. 1c–1h. The Fe-Cr-Ni alloy substrates and stainless-steel cathode are submerged in 20 ml H_2SO_4 electrolyte filled in a Pyrex beaker, as shown in Fig. 1c. Fe-Cr-Ni alloy cylinder connected to the Pt anode and stainless-steel rod attached to the cathode of the DC power supply (Keysight E3649A dual output) completed the electrical circuit. The external potential resulted in the oxidation reaction at the anode and the reduction reaction at the cathode, as shown in Fig. 1d.

A cross-sectional view of the electrode arrangement and the electrolyte chemistry are presented in Fig. 1e. Several species, such as water molecules, H^+, OH^-, M^{n+} (metal ions), and SO_4^{-2}(sulfate ions), are generated in the electrolyte. Sulfate ions are responsible for metal dissolution, while water molecules oxidize the metal surface (Fig. 1d). A viscous film comprising dissolved oxidation

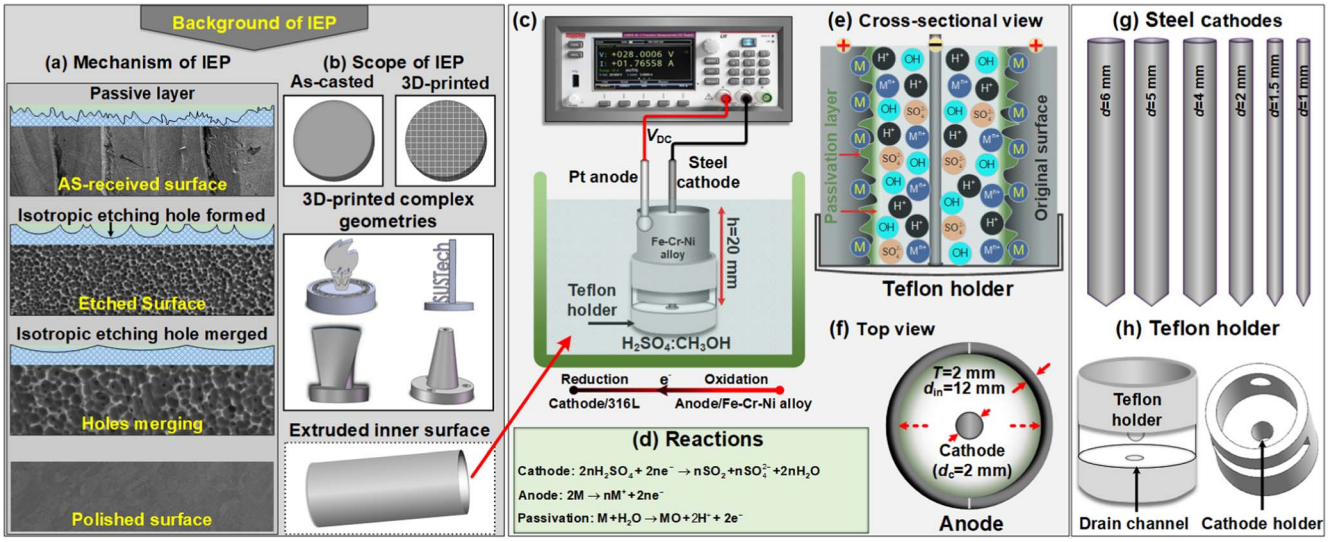

Figure 1. Background of isotropic etching polishing, mechanism of IEP (a), the scope of IEP (b), schematic of the experimental setup of the IEP of Fe-Cr-Ni alloy cylinder inner surface in 20 ml H_2SO_4 electrolyte (c), chemical reactions occurring at anode and cathode (d), the cross-sectional view (e), the top view (f), steel cathodes with different diameters (g), and Teflon holder viewed from different angles (h).

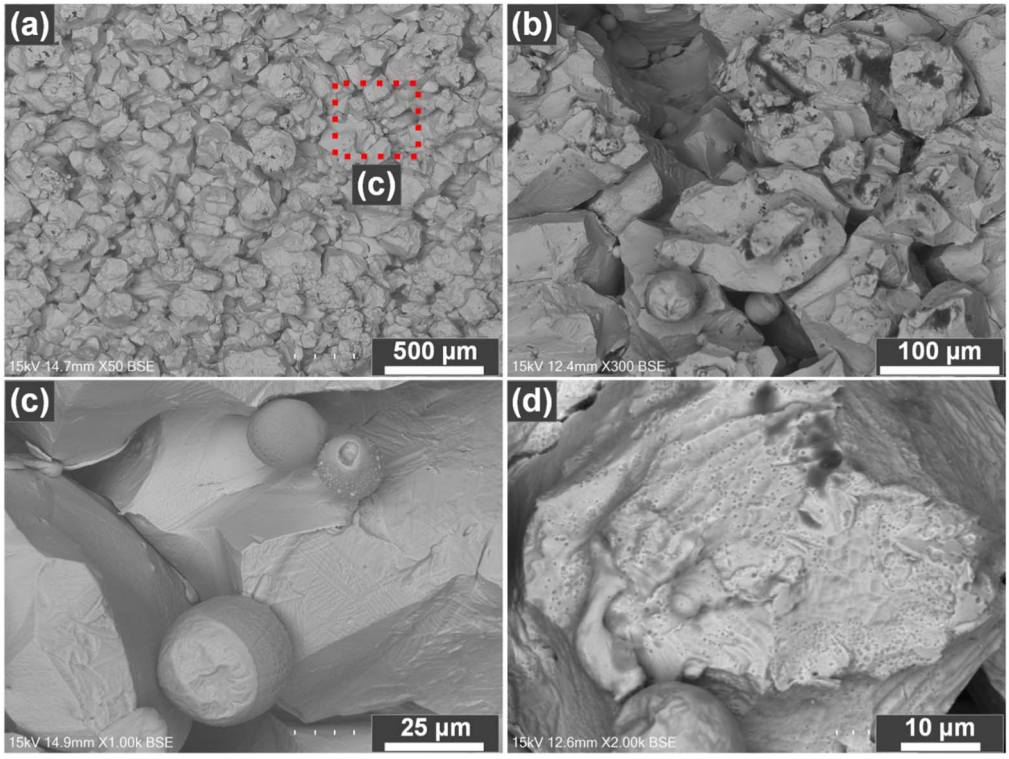

Figure 2. SEM morphologies of the as-extruded Fe-Cr-Ni alloy inner surface at different positions, large area morphology (a), deep valleys and sharp protrusions (b), weakly attached powder particles (c), and porosity (d).

products develops on the surface, whose electrical resistance depends on its thickness. The viscous film is more resistive and thick in valleys than at protrusions, as shown by the green-colored gradient in Fig. 1e. As discussed, the IEP initiates with the breaking of the passivation layer, which is increasingly plausible in the protruding regions due to the high current density (discussed in section 3.2). Eventually, the surface protrusions are dissolved, and surface leveling is achieved due to the isotropic etching holes formation and merging.

The top view of the electrode arrangement is projected in Fig. 1f, highlighting the dimensions of the anode and cathode and the gap between them. Similarly, steel cathodes with different diameters and the Teflon holder used in this study are shown in Figs. 1g and 1h, respectively. Teflon holder is designed such that the upper circular strips can grip axially sectioned electrodes in a cylindrical shape, while the drain channel allows the exchange of electrolytes that also sweeps away the dissolved metal ions and heat generated during the electrochemical process. In the absence of a drain channel, dissolved metal ions and generated heat will be trapped in the cavity, significantly deteriorating the electrochemical polishing process. A hole in the bottom of the Teflon holder was specially designed to vertically align the cathode at the center of the cylinder for electric field invariability.

Material characterization.—The inner surface morphologies of the axially sectioned cylindrical samples before and after processing were recorded by a scanning electron microscope (SEM, Hitachi TM4000Plus). In addition, compositions of the as-extruded and polished Fe-Cr-Ni alloy substrates were determined by the Energy Dispersive X-ray Spectroscopy (EDS) connected with the SEM. Compositions of the Fe-Cr-Ni alloy as-extruded and polished for 2 min are given in Table I. Two compositions are comparable, except for a considerable reduction in the oxygen composition after polishing. Iron is the most abundant element (>50%) in the alloy, and iron rusting can be the primary source of oxygen bonding to the surface. As a result of polishing for 2 min, the oxygen content was appreciably reduced, as was the iron rusting.

Table I. Chemical composition (wt%) of the as-extruded and polished Fe-Cr-Ni alloy.

Element	Ni	Cr	Fe	C	Al	Si	Mn	O
As-extruded	17.8	23.7	50.5	4.3	0.3	0.6	1.0	2.5
IEP 2 min	18.8	24.2	52.5	2.1	0.8	0.1	0.7	0.7

The average surface roughness (Sa roughness) is an extensively studied universal parameter describing shapes and distributions of irregularities.[22] The Sa roughness was determined by the scanning white light interferometer (WLI, CCI HD, Taylor Hobson) over an area of 400 × 400 μm^2 after processing WLI images at 80 μm cutoff wavelength and 2nd order flattening. Similarly, the profilometer (SURFCOM NEX 031 DX-12) measured the surface profiles and the average line roughness (Ra roughness) over a constant length of 15 mm. Finally, the volumetric MRR was calculated from the mass difference determined by the digital precision balance (Mettler XSR105).

Current efficiency.—The theoretical mass of the electrochemical dissolution of metals can be calculated from Faraday′s law. Typically, the theoretically calculated dissolution mass is not consistent with the experimentally dissolved mass, which institutes the concept of current efficiency. For example, a current efficiency of <100% evinces metal dissolution accompanied by possible side reactions, while a current efficiency of > 100% insinuates peeling off metal lumps in place of electrochemical metal dissolution. The current efficiency (η) is defined as follows:

$$\eta(\%) = \frac{\Delta m_{\text{diss}}}{\Delta m_{\text{theo}}} \times 100 = \frac{\Delta m_{\text{diss}}}{kIt} \times 100 \qquad [1]$$

where Δm_{diss} is the mass (g) experimentally dissolved during electrochemical polishing of metals or alloys, and Δm_{theo} is

theoretically calculated mass (g) dissolved based on Faraday's law. The theoretical mass dissolved is further defined as kIt in Eq. 5; where k is theoretical mass equivalent (g/As), I is the constant current (A) applied during electrochemical polishing time t(s). For an alloy, k is defined as follows:

$$k = \frac{1}{F\left(\frac{n_1}{A_1}a_1 + \frac{n_2}{A_2}a_2 + \frac{n_3}{A_3}a_3 + ...+\frac{n_x}{A_x}a_x\right)} \quad [2]$$

where Faraday constant is $F = 96500\,\mathrm{C\,mol^{-1}}$, n_x is the valency of the dissolved element, A_x is the relative atomic mass (g $\mathrm{mol^{-1}}$), and a_x is the percentage concentration of an element in the alloy.

Current efficiency in this study was calculated as a function of the cathode thickness (1, 1.5, 2, 4, 5, and 6 mm) that outcomes in the variation of electrode gap; applied current (0.1, 0.5, 1, 1.5, 2, 2.5, and 3 A) that modulates the current density and metal dissolution rate; and the polishing duration. In addition, only the key constituents (Fe, Cr, and Ni) that account for more than 95% of the recipe were used in the current efficiency calculation of the IEP of Fe-Cr-Ni alloy.

Surface hardness.—The nanoindentation experiments measured Vickers hardness of the as-extruded and grinded Fe-Cr-Ni alloy inner surface before and after polishing. Two different Fe-Cr-Ni alloy substrates were simultaneously polished such that one cross-sectioned half of the cylinder was as-extruded while the other half was grinded. Both parts were fastened together by a Teflon holder and polished at a constant current of 3 A for 10 min in 20 ml H_2SO_4 electrolyte. The polished parts were ultrasonically washed in ethanol absolute and de-ionized water for 10 min each and then blow-dried. Since the original substrates were curved and did not support the inner surface nanoindentation measurements, the as-extruded, grinded, and polished substrates were cut into small pieces using wire electric discharge machining (WEDM). The WEDM cut substrates were ultrasonically rewashed to remove any debris on the surface. Later, the Hysitron Ti-950 was used to measure the Vickers hardness of the as-extruded and processed substrates by loading, holding, and unloading 1000 μN force each for 10 s.

Results and Discussions

As-extruded Fe-Cr-Ni alloy surface morphology.—Surface morphologies of the as-extruded Fe-Cr-Ni alloy cylinder at different positions and magnifications (X50, X300, X1000, and X2000) are shown in Fig. 2. The as-extruded surface appears extremely rough due to numerous protrusions, deep valleys, attached and trapped powder particles, and iron rusting, as shown in Fig. 2a. Deep valleys, sharp protrusions, and powder particles are more evident when the surface morphology is recorded at higher magnification (Fig. 2b). Unlike the AM of metals, where powder particles bond to the surface during the melting phase of the bulk[23]; a small proportion of the powder particles are seen bonding to the as-extruded substrate surface (Fig. 2c), and the rest are pushed and trapped into valleys, as observed in Fig. 2b. A proportion of these particles is released during ultrasonic cleaning, while the rest are either electrochemically dissolved or fall off with metal lumps removal or dissolution. In addition, surface porosity was observed in some regions of the as-extruded Fe-Cr-Ni alloy (Fig. 2d) that can significantly deteriorate the surface corrosion resistance aside from the powder particles attached to the surface.[24] High surface roughness of the as-extruded inner surface strongly depends on the extrusion parameters such as forming load, contact surface enlargement, the sliding distance between the substrate in the die, operating temperature, and the normal pressure.[4] In addition, surface defects generated during the extrusion also worsened the surface roughness.[5]

Electric field simulation.—Typically, the as-received surfaces contain protrudes, valleys, and powder particles that affect passivation layer thickness and the local dissolution rate. The as-extruded Fe-Cr-Ni alloy surface exhibits similar features that lead to overall poor morphology, as shown in Figs. 2a–2d. Besides, instantaneous morphology changes due to falling off metal lumps and trapped powder particles during surface polishing significantly affect the planarization efficiency and final surface uniformity. Therefore, electric field simulation over a model surface, replicating various original surface features, is essential for electric field distribution and insights related to metal dissolution in different regions. The model surface was designed with protrusions, valleys, and flat areas, as shown in Fig. 3. While maintaining the generality of the process, the simulation was simplified based on two assumptions. (i) The anode and cathode were taken as equipotential surfaces, and the distribution of current flowing between them was based on Ohm′s law. Besides, the current distribution was entirely determined by the primary current. (ii) The electrolyte was supposed to be ideal, having a uniform concentration, temperature, and conductivity distribution.

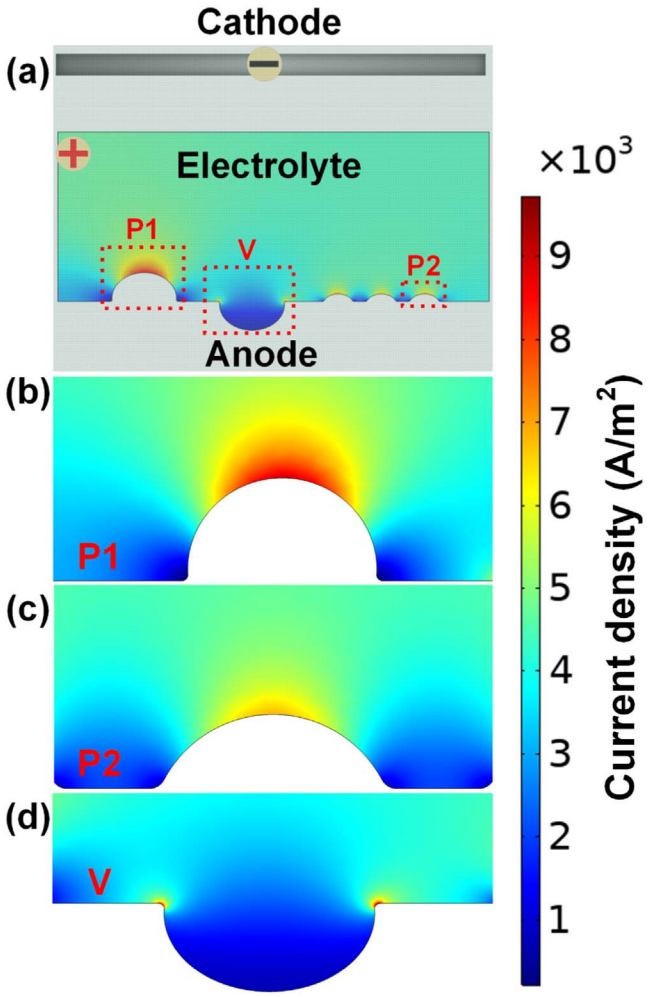

Figure 3. Current density distribution at different regions of the model surface.

The electric potential (V) of the electrolyte based on the electric field theory is given by Laplace's equation:

$$\nabla^2 V = \frac{\partial^2 V}{\partial^2 x^2} + \frac{\partial^2 V}{\partial^2 y^2} = 0 \quad [3]$$

Based on Ohm's law, the current density (J) is given as:

$$J = -\lambda \nabla V \quad [4]$$

where λ denotes the uniform electrical conductivity of the electrolyte.

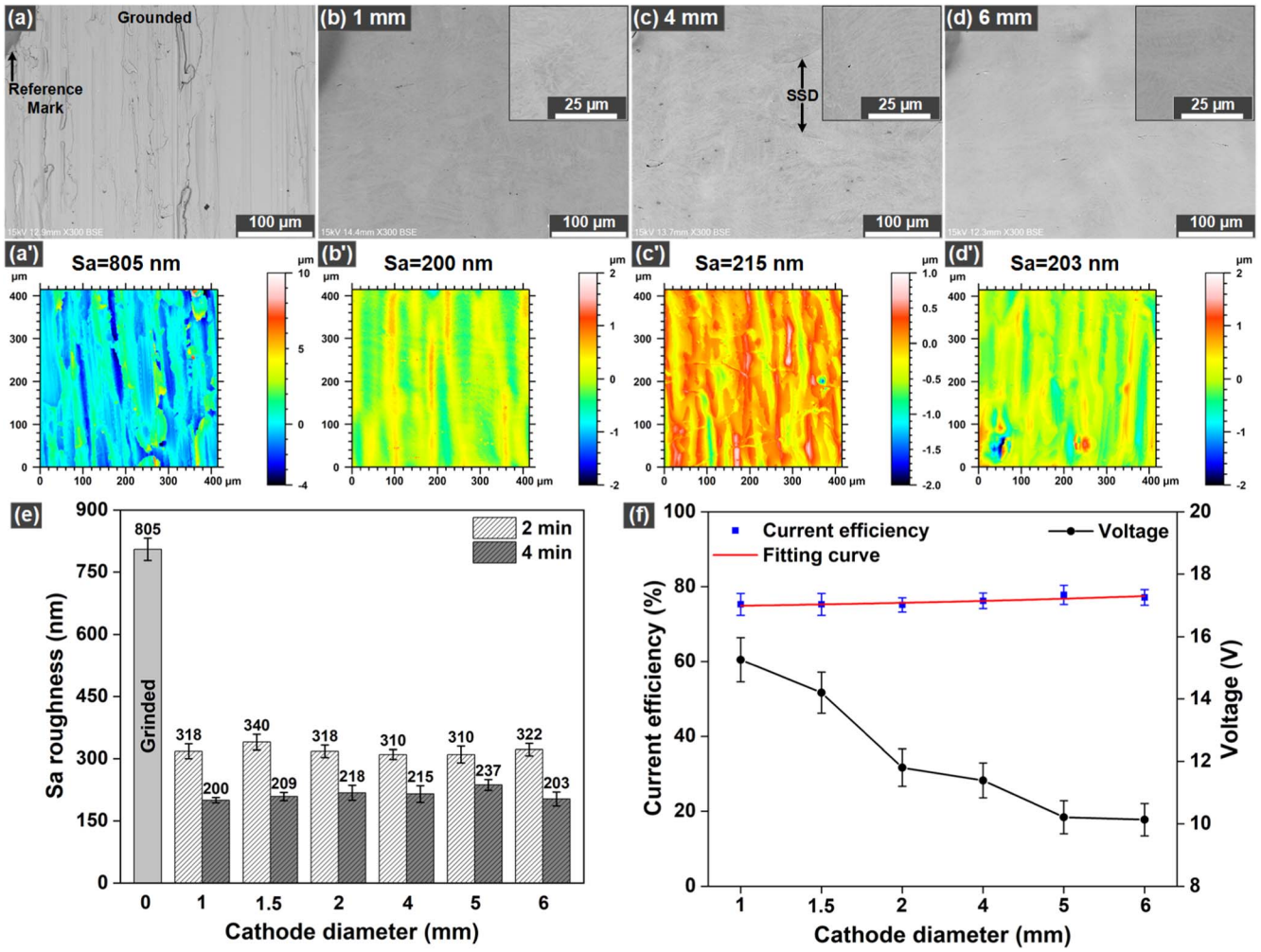

Figure 4. Variations in the surface morphologies (a-d), WLI morphologies (a′)–(d′), and Sa roughness (e) of the grinded Fe-Cr-Ni alloy cylinder inner surface, and changes in the current efficiency and required voltage (f) of IEP conducted for 2 and 4 min at 0.31 A cm^{-2} in 20 ml H_2SO_4 electrolyte with increasing cathode diameter (1, 1.5, 2, 4, 5, and 6 mm).

Based on the electric field simulation, the following boundary conditions are imposed:

$$V\,|\Gamma_{anode} = \mathrm{U} \qquad [5]$$

$$V\,|\Gamma_{cathode} = 0 \qquad [6]$$

where U denotes the constant potential both on the internal and external surfaces of the anode. COMSOL Multiphysics (5.3 v) was used to run the simulation, which finely meshed model domains with triangular elements to ensure accurate results.

The electric field simulation results of the model surface representing Fe-Cr-Ni alloy are shown in Fig. 3a. The current density drastically varied between the characteristic regions. For example, the current density at the highest protrusion (P1) is maximum (Fig. 3b) and markedly reduced at P2 (Fig. 3c), whose height is much shorter than P1. The current density in flat regions is comparatively moderate and dropped to a minimum in the valley (V) region (Fig. 3d). The simulation proposed a relatively higher current density distribution at the protruding areas, which conforms with the inverse square law of the electric field. The high current density can promote vigorous dissolution of protrusions during electrochemical polishing.

Effect of cathode diameter and current on IEP of Fe-Cr-Ni alloy.—Apparently, the gap between working electrodes should significantly affect the planarization efficiency during electrochemical polishing since the electric field follows the inverse square law of the distance between the anode and cathode. Since the cylindrical anode has a fixed inner diameter of 12 mm, the gap between the anode and cathode decreases accordingly with increasing cathode diameter. Therefore, the IEP was conducted for 2 and 4 min in 20 ml H_2SO_4 electrolytes at a constant current density of 0.31 A cm^{-2} with steel cathode diameters varying (1, 1.5, 2, 4, 5, and 6 mm), and the results are shown in Fig. 4. As discussed, falling off metal lumps and powder particles could create discrepancies in the final Sa roughness and material removed. That is why grinded Fe-Cr-Ni alloy substrates were used in these experiments. Inner surface SEM morphologies and WLI profiles of the grinded and polished Fe-Cr-Ni alloy substrates are shown in Figs. 4a–4d and 4a′–4d′, respectively. It can be seen that the roughly grinded Fe-Cr-Ni alloy inner surface turns relatively smooth after the IEP for 4 min removes surface grinding marks, which is also obvious from the high magnification insets in Figs. 4b–4d. However, several subsurface damages originating during the extrusion process can be observed on the polished surface, which significantly deteriorates the surface quality. Figure 4e shows improvement in the Sa roughness after polishing the grinded Fe-Cr-Ni alloy substrate (Sa = 805 nm) for 2 and 4 min. For different cathode diameters, the final Sa roughness values after 2 and 4 min of IEP remain monotonous. A standard deviation of 10 ∼ 12 nm calculated from the Sa roughness values shows that results are highly repetitive, and cathode diameter did not affect the IEP

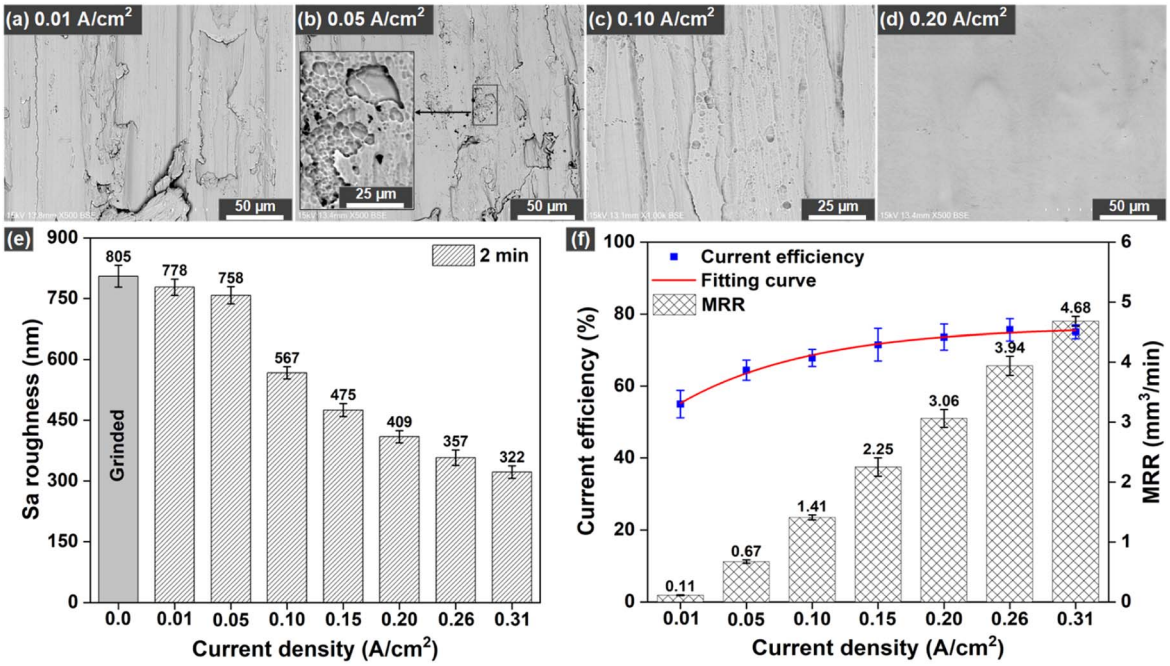

Figure 5. Variations in the surface morphologies (a-d), and Sa roughness (e), of the grinded Fe-Cr-Ni alloy cylinder inner surface, and changes in the current efficiency and MRR (f) of IEP conducted for 2 min in 20 ml H_2SO_4 electrolyte with 2 mm cathode diameter and increasing applied current density (0.01, 0.05, 0.10,0.15, 0.20, 0.26, and 0.31 A cm^{-2}).

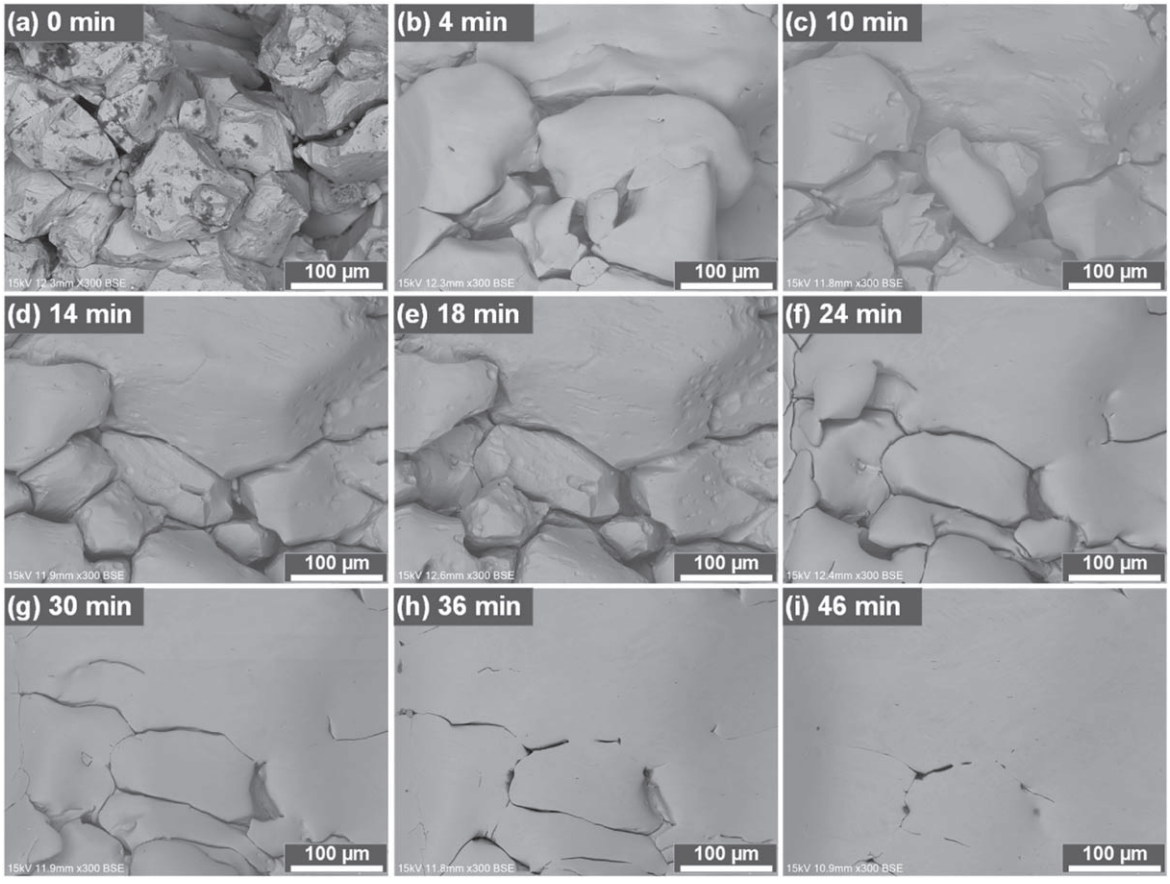

Figure 6. SEM morphologies of the inner surface of as-extruded Fe-Cr-Ni alloy polished in 20 ml H_2SO_4 electrolyte at 3 A current with 2 mm cathode diameter for different durations (0–46 min).

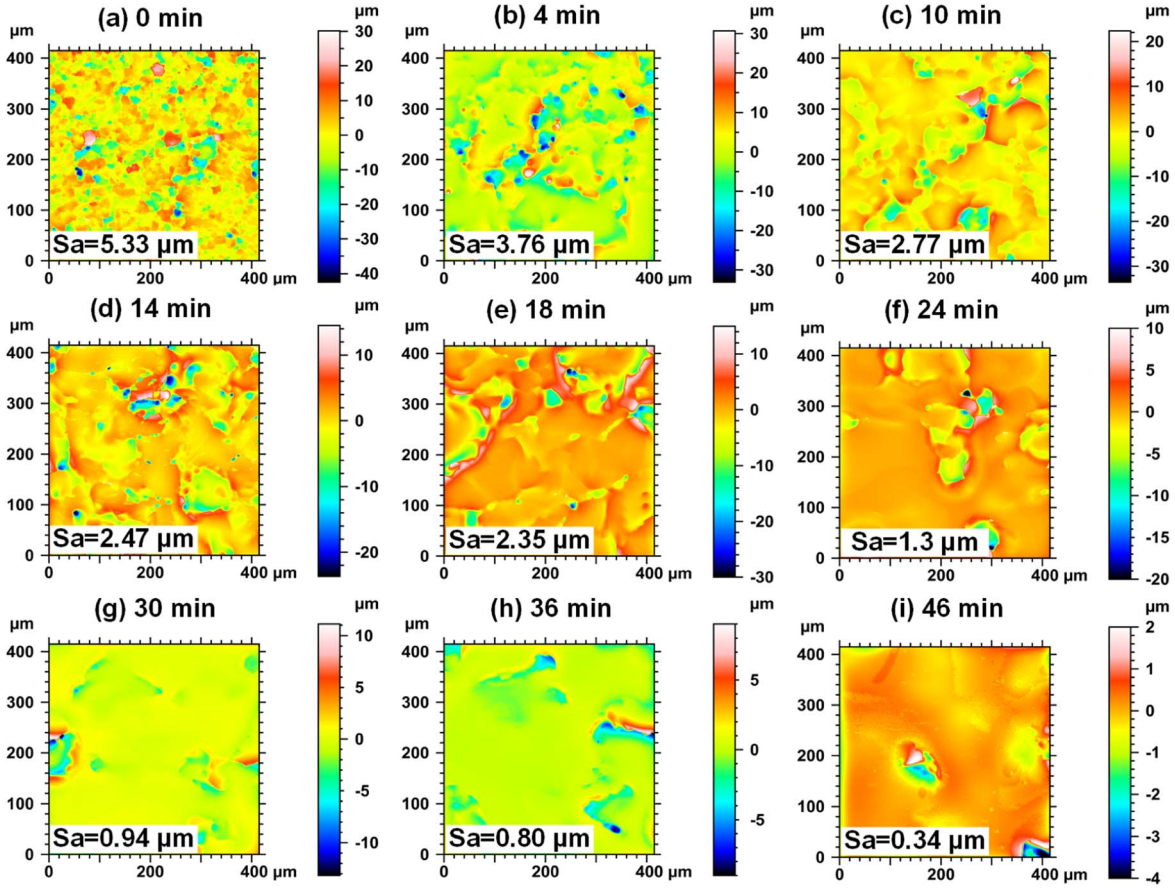

Figure 7. WLI morphologies of the inner surface of as-extruded Fe-Cr-Ni alloy polished in 20 ml H_2SO_4 electrolyte at 3 A current with 2 mm cathode diameter for different durations (0–46 min).

process. The current efficiency calculation further supports the results and recording of the required voltage to sustain 0.31 A cm^{-2} current density, as shown in Fig. 4f. Similar to the Sa roughness trend, the current efficiency remains tedious, while the required voltage to sustain 0.31 A cm^{-2} current density decreases with increasing cathode diameter. Although a relatively high power dissipation can be expected at a high applied voltage, that may affect the current efficiency. However, a monotonous trend of current efficiency shows that the dissipated heat was efficiently released to the bulk of electrolyte from the Teflon holder drain, and the average increase in the electrolyte temperature was not very high. It is because the high concentrations of H^+ and SO_4^{-2} ions substantially increase electrolyte conductivity and sponsor heat flow from the anode to the bulk of the electrolyte. The preceding discussion concludes that the cathode diameter does not affect the current efficiency and planarization efficiency of IEP unless the applied current is constant, which is consistent with Faraday′s law.

As discussed, the planarization and current efficiencies remained monotonous when the applied current density was kept constant; therefore, the effect of applied current density was also investigated on IEP. In these experiments, the IEP was conducted in 20 ml H_2SO_4 electrolytes for 2 min, keeping the cathode diameter fixed at 2 mm and systematically increasing the applied current density from 0.01 A cm^{-2} to 0.31 A cm^{-2}. The results are shown in Fig. 5. The SEM morphologies of the inner surface polished for 2 min at 0.01 A cm^{-2} (Fig. 5a) and 0.05 A cm^{-2} (Fig. 5b) showed no improvement in the surface morphologies. Sharp grinding marks similar to the initially grinded substrate (Fig. 4a) were still noticeable. However, unlike 0.01 A cm^{-2}, some etching sites on the Fe-Cr-Ni alloy inner surface were observed at 0.05 A cm^{-2}, which is evident from the high-resolution inset in Fig. 5b. According to the mechanism of IEP, a passivation layer develops at the metal surface that breaks down when the applied current density is appropriate.[18] The etching hole density increases with the applied current density, which is evident from Fig. 5c, where the density of the holes drastically increases, and many of them are seen merging at 0.1 A cm^{-2}. Besides, some of the etching holes are larger in diameter, attributed to the random breakdown of the passivation layer. Some etching holes can grow faster than others under local high-temperature conditions.[25] Typically, high current density can produce large heat dissipation, raising the anode temperature higher than the bulk of electrolyte. When IEP was conducted at 0.20 A cm^{-2}, all the etching holes merged within 2 min, and a new surface evolved with very faint impressions of peaks and valleys. Further increasing current density while keeping the rest of the conditions constant produced even better surfaces. It shows that higher current density facilitates vigorous etching and accelerates planarization efficiency.

Variation in the Sa roughness of the grinded Fe-Cr-Ni alloy inner surfaces after IEP for 2 min in 20 ml H_2SO_4 electrolytes at different current densities (0.01 A cm^{-2} to 0.31 A cm^{-2}) is shown in Fig. 5e. The Sa roughness after IEP up to 0.05 A cm^{-2} did not change since the current density was very low, and the surface etching was hardly observed. This is also obvious from the SEM morphologies in Figs. 5a, 5b. Although extensive etching holes merging can be seen in Fig. 5c and the Sa roughness significantly drops after etching at 0.10 A cm^{-2}, it is still very high (567 nm), possibly due to the large diameter etching holes and considerable height difference between peaks and valleys on the surface. After that, the Sa roughness decreased consistently. For example, after IEP at 0.20 A cm^{-2}, a new surface unfolded following the etching holes merging. However, a relatively longer polishing time was necessary to obtain a high-quality mirror-like surface. Respectively, we can conclude

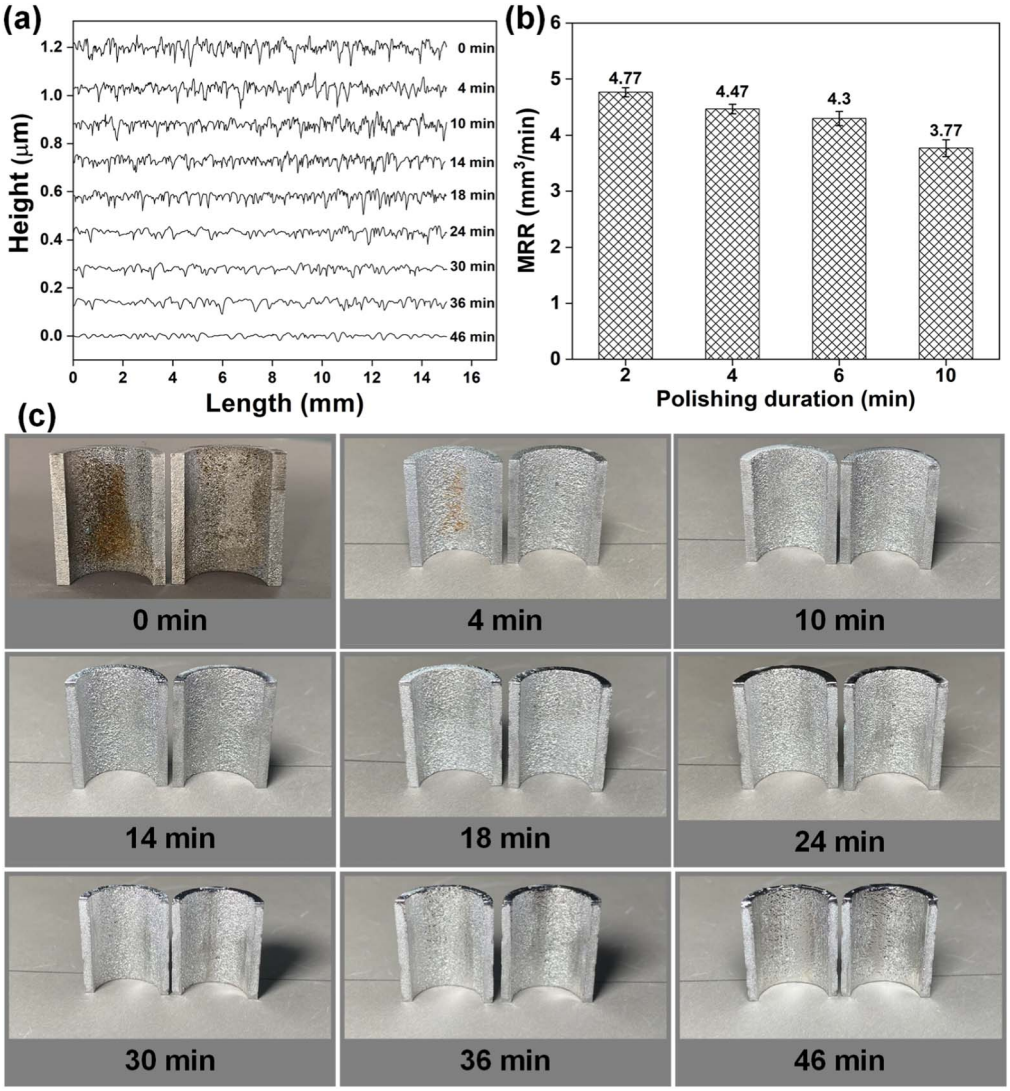

Figure 8. Surface profiles (a), MRR (b), and images (c) of the as-extruded Fe-Cr-Ni alloy inner surface polished in 20 ml H_2SO_4 electrolyte at 3 A current with 2 mm cathode diameter for different durations (0–46 min).

that IEP has different stages: (i) passivation begins with metallic substrate immersing in the IEP electrolyte, (ii) isotropic etching begins with appropriate current density, (iii) isotropic etching holes merge and unfold a new surface, and (iv) polishing when etching hole grows extremely large in diameter, and the Sa roughness decreases steadily.

In addition, current efficiency and MRR are calculated as a function of the increasing current density, as shown in Fig. 5f. The current efficiency is minimum at 0.01 A cm^{-2}, initially increasing exponentially with the applied current and steadily after 0.20 A cm^{-2}. The current density at 0.01 A cm^{-2} is not high enough to break the passivation layer, and the metal dissolution and material removal remain minimal. Ohmic losses in the acidic systems are high because the passivation layer development on the electrodes decreases the current efficiency.[26] However, the current efficiency at 0.05 A cm^{-2} increases significantly, which is related to the breakdown of the passivation layer and the formation of isotropic etching holes on the Fe-Cr-Ni alloy inner surface. Passivation layer breakdown and formation of isotropic etching holes is a generic attribute of IEP that remarkably adds to its finishing efficiency. An increase in the current efficiency with applied current density has been observed and attributed to the passivation layer breakdown when investigating electrochemical machining of mild steel in $NaNO_3$ electrolyte.[27] A high current density produces more heat, raises the temperature of the substrate, and decreases the viscosity of electrolytes, ultimately improving the current efficiency.[28] The current efficiency becomes steady after 0.20 A cm^{-2}, possibly due to excessive side reactions, such as the oxygen gas evolution reaction ($2O^{2-} \rightarrow O_2 + 4e^-$),[29] and the formation of $Cr_2O_7^{2-}$.[30] Similarly, the MRR increases with current density, showing that IEP becomes more efficient at higher current density. However, when applied current density increases, the MRR increases rapidly at low current density and steadily at high current density. For example, the MRR increases nearly 6 times when the applied current density increases from 0.01 to 0.05 A cm^{-2} but only 1.2 times when the current density increases from 0.26 to 0.31 A cm^{-2}. The increasing trend of MRR is also consistent with the current efficiency and surface planarization efficiency.

Polishing characteristics of the as-extruded Fe-Cr-Ni alloy.—It has been established that the overall efficiency, including current and planarization efficiency and MRR, increases with the applied current, while cathode diameter does not affect the planarization efficiency. Therefore, the subsequent experiments are conducted in 20 ml H_2SO_4 electrolyte at 3 A with a 2 mm cathode.

In these experiments, the inner surface morphology evolution of the as-extruded Fe-Cr-Ni alloy is investigated, and the results are

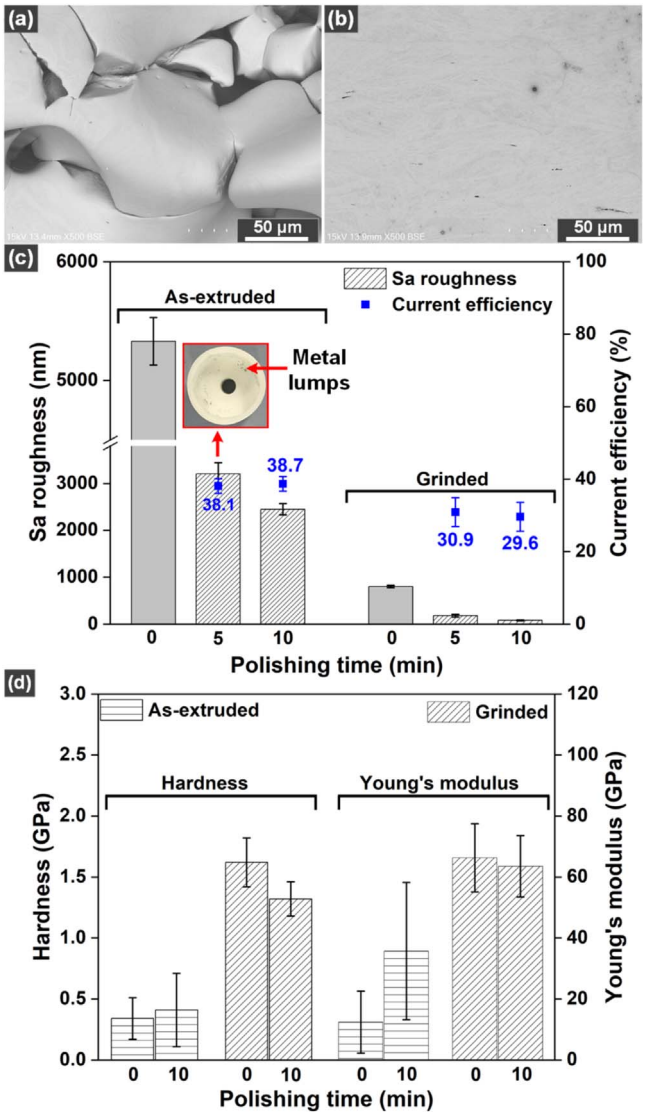

Figure 9. SEM morphologies of the as-extruded (a) and grinded (b) Fe-Cr-Ni alloy substrates, Sa roughness and current efficiencies (c), and surface hardness and Young's modulus (d) after polishing up to 10 min in 20 ml H_2SO_4 electrolyte at 3 A with 2 mm cathode diameter.

shown in Fig. 6. The shallow passivation layer is relatively easy to break at high current density, promoting rapid dissolution at the protruding areas. Similar behavior is observed when the as-extruded surface is polished for 4 min. Sharp protruding regions become relatively flat, and the valleys become shallow. Besides, the weakly attached metal lumps are detached from the surface due to the dissolution of necking regions. Apparent detachment of band protrusions can be observed between 10–14 min of IEP, which resulted in the evolution of whole new inner surface morphology, as shown in Figs. 6c–6d. Hence, for a highly rough surface, it is not only the initial surface condition that influences the post finishing surface morphology and polishing duration but also the band protrusions that instantaneously break from the surface and significantly revamp the surface morphology, current distribution, and possibly the passivation layer during polishing. In addition, isotropic etching hole formation and merging can also be seen between 10 to 18 min, which may be formed due to passivation layer disturbance during instant morphology changes with metal lumps dropping. After polishing up to 24 min, obvious surface flattening is realized, which keeps improving as IEP progresses. Polishing for up to 46 min dissolved all the protrusions, and a flat surface with significantly enhanced quality was realized. Still, some micro-sized deep valleys between flat regions were observed, demonstrating that extrude has poor build quality.

The WLI morphologies of the as-extruded Fe-Cr-Ni alloy after IEP for different durations are shown in Fig. 7. The WLI profile of the as-extruded Fe-Cr-Ni alloy contained many protrudes and valleys varying from 30–40 μm in height, as seen in Fig. 7a. Sharp protrudes were dissolved, valleys became shallow ($\sim$30 μm), and the initial Sa roughness of 5.33 μm was reduced to 3.76 μm after IEP for 4 min (Fig. 7b). After polishing for 10 min (Fig. 7c), flat boundaries emerged, and the polished area increased significantly. This trend continued up to 24 min (Fig. 7f), where the extensive merging of flattened regions was observed. The effective size of flattened regions considerably increased compared to valleys, and the Sa roughness was reduced to 0.34 μm after 46 min of IEP (Fig. 7i). Although the Sa roughness was reduced by $\sim$93%, it was still decreasing linearly, indicating that the limiting Sa roughness was not reached, possibly due to the generation of miniaturized deep valleys during the extrusion manufacturing.

The Fe-Cr-Ni alloy inner surfaces were further characterized for surface profiles, material removal rate, and images, as shown in Fig. 8. The surface profile of the as-extruded substrate was exceedingly rough due to high protrusions and deep valleys, as shown in Fig. 8a. The line profiles kept gradually smoothing as IEP progressed. After IEP up to 18 min, the surface profiles did not significantly improve due to randomly breaking alloy lumps inducing severe changes in the surface morphology. The surface quality was considerably enhanced after 24 min of IEP, and the surface profile became relatively smooth after flattening band protrusions. The surface profile measured after 24 min of IEP also endorsed the morphologies of Fe-Cr-Ni alloy obtained from SEM (Fig. 6f) and WLI (Fig. 7f). An exceptionally smooth profile with short protrusions and shallow valleys was obtained after polishing for 46 min. The variation in MRR with different polishing intervals is shown in Fig. 8b. Highest MRR was obtained for 2 min interval, which slightly decreased with increasing the polishing interval. A high MRR in the initial polishing stage can be related to removing powder particles and breaking band protrusions from the substrate surface. Later, the MRR was only based on the dissolving protrusions and slightly decreased with improving surface quality. The MRR trend is consistent with the improving surface quality of the as-extruded Fe-Cr-Ni alloy substrate with polishing. Figure 8c shows a highly rough and rusty as-extruded Fe-Cr-Ni alloy surface gradually turning smooth and shiny after each IEP experiment. It is to be mentioned that no significant polishing effects were observed on the outer surface of the substrate.

Simultaneous polishing of as-extruded and grinded Fe-Cr-Ni alloy.—Typically, electrochemical-based polishing methods can produce mirror-like surfaces of metals and alloys. However, polishing extremely rough surfaces with instantly varying surface morphologies due to dropping off metal lumps is seriously challenging and requires a very long polishing time, as observed in section 3.3. In addition, the inconsistent surface quality of as-extrudes processed by a single manufacturing method is particularly problematic, while the uniform distribution of Sa roughness is equally desired compared to low Sa roughness. Therefore, the as-extruded and grinded Fe-Cr-Ni alloy substrates are simultaneously polished via IEP to compare changes in their morphology, Sa roughness, current efficiency, and surface mechanical properties such as hardness and Young's modulus.

The as-extruded Fe-Cr-Ni alloy inner surface morphology (Fig. 9a) is highly non-uniform compared with the grinded substrate (Fig. 9b) after polishing for 10 min. The highly non-uniform inner surface morphology of the as-extruded substrate after IEP is still inherited from the initial surface condition described in section 3.1. Although the dissolution of protruding areas is more probable in electrochemical finishing, as discussed in section 3.2, falling off metal lumps causes instant changes in surface morphology and

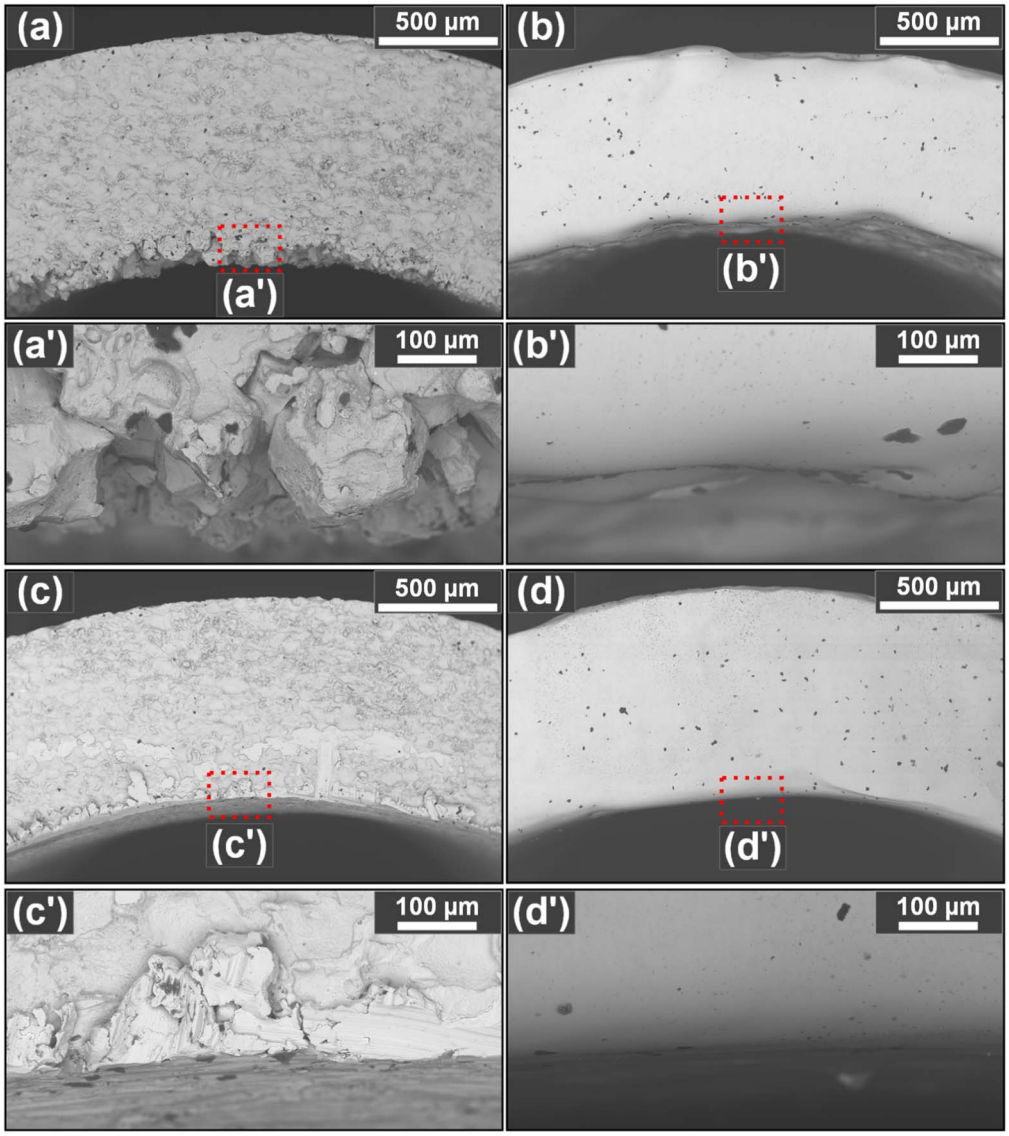

Figure 10. Inner edges and wall thickness of the as-extruded (a), (a′) and polished for 46 min (b), (b′), and grinded (c), (c′) and polished for 10 min (d), (d′) in 20 ml H_2SO_4 electrolyte at 3 A with 2 mm cathode diameter.

strongly influences the current distribution and final surface quality. In contrast, grinding can mechanically eliminate metal lumps and powder particles from the Fe-Cr-Ni alloy inner surface. At the same time, IEP can produce a smooth surface even after polishing for a short duration of 10 min.

Changes in the Sa roughness and current efficiency of simultaneously polished as-extruded and grinded Fe-Cr-Ni alloy substrates are shown in Fig. 9c. Although the inner surface Sa roughness decreases for both as-extruded and grinded substrates after polishing for 5 and 10 min, the planarization efficiency, defined as the percentage reduction in the Sa roughness, is up to 37% more for the latter than its counterpart after IEP up to 10 min under the same conditions. Moreover, the as-extruded inner surface Sa roughness standard deviation is exceptionally higher than the grinded substrate, showing that the latter has a very uniform Sa roughness distribution after polishing. In contrast, the current efficiency of the as-extruded substrate (∼38%) remains higher than the grinded substrate (∼30.9%) after polishing 10 min, which, in addition to the typical electrochemical metal dissolution, is an indication of metal lumps falling. The dropped-off metal lumps accumulated at the bottom of the Teflon holder can be seen in the inset Fig. 9c.

The surface hardness and Young′s modulus of the as-extruded and grinded Fe-Cr-Ni alloy substrates after simultaneously polishing for 10 min are shown in Fig. 9d. On the one hand, the surface hardness and Young's modulus of the as-extruded substrate increased with grinding and polishing. On the other hand, it slightly decreased after the IEP of the grinded substrate. Variation in the mechanical properties with grinding is closely related to the stress introduced by the typical mechanical grinding process.[31] Similarly, the thickening of the surface layer with grinding increases the surface hardness.[32] Besides, improved surface uniformity with IEP enhanced the surface mechanical properties of the as-extruded surface since the nanoindenter measures these values relative to the first contact with the target surface, and finishing improves the surface contact area by removing voids on the as-extruded rough surface. Xia et al.[33] found a strong dependence of mechanical properties on the Sa roughness. However, a slight reduction in the surface hardness and Young′s modulus after IEP is related to removing stress from the surface. Since electrochemical polishing methods are good at eliminating stress introduced by mechanical grinding and thinning of surface layer.[32] Nevertheless, improving surface corrosion properties with electrochemical polishing that

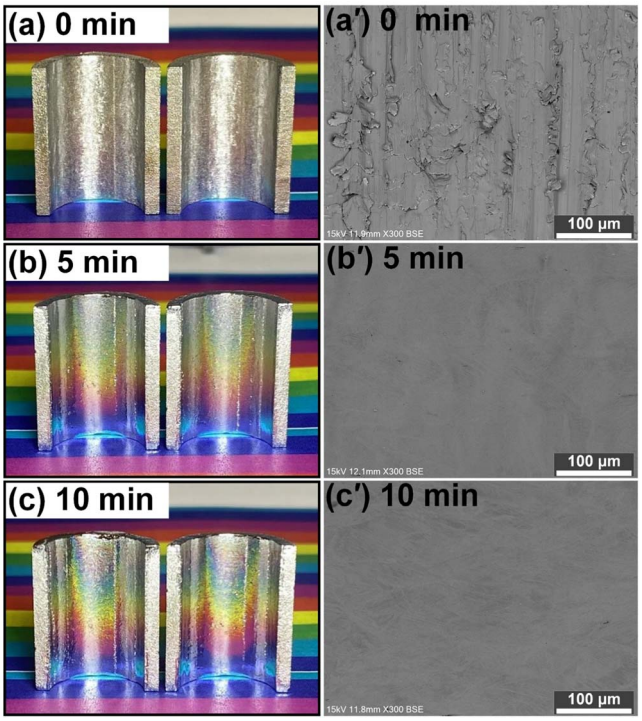

Figure 11. Images and SEM morphologies of the grinded Fe-Cr-Ni alloy (a), (a′), polished for 5 min (b), (b′), and 10 min (c), (c′) in 20 ml H_2SO_4 electrolyte at 3 A with 2 mm cathode diameter.

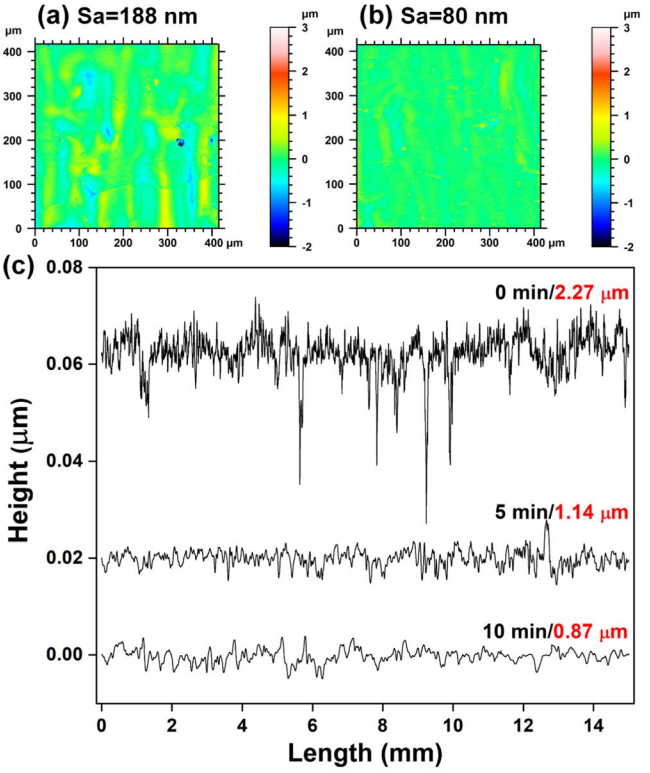

Figure 12. WLI morphologies of the inner surface of grinded Fe-Cr-Ni alloy polished for 5 min (a), 10 min (b), and line profiles and Ra roughness (c).

reduces surface porosity, stress, and Sa roughness is a good tradeoff with a slight reduction in mechanical properties.[34] Excellent mechanical properties are one of the fundamental prerequisites in metal applications. In conclusion, initial morphology and metal lumps removal during electrochemical polishing strongly influence the final surface morphology, Sa roughness, and surface mechanical properties. Besides, the IEP of the mechanically grinded Fe-Cr-Ni alloy inner surface dramatically improves the final surface quality, Sa roughness uniformity, planarization efficiency, and surface mechanical properties, which is strongly desired in practical applications of metals and alloys.

Furthermore, the morphology of the edges and wall thickness of the as-extruded Fe-Cr-Ni alloy substrate polished for 46 min (discussed in section 3.4) are compared with the grinded substrate polished for 10 min, as shown in Fig. 10. The as-extruded Fe-Cr-Ni alloy substrate (Fig. 10(a, a′)) inner edge is highly rough and non-uniform due to excessive band protrusions compared with the grinded substrate (Figs. 10c, 10c′), which appears relatively less rough under SEM. Although, protrusions on the inner edges of both the substrates are dissolved after polishing for different durations. Still, edges in the case of the grinded substrate (Figs. 10d, 10d′) are markedly sharp and uniform than the as-extruded substrate (Figs. 10b, 10b′) polished for a longer duration. The wall thickness of the grinded Fe-Cr-Ni alloy substrate after polishing for 10 min is reduced by only 6%, while that polished for 46 min decreased by 25% compared with the as-extruded Fe-Cr-Ni alloy substrate. Thus, the IEP of the grinded Fe-Cr-Ni alloy substrate realized a better and uniform inner surface with larger wall thickness and smooth edges, which is desirable for functional inner surfaces for a smooth and uninterrupted supply of liquid and gases.

Polishing characteristics of the grinded Fe-Cr-Ni alloy.—It has been established that as-extruded Fe-Cr-Ni alloy inner surface polishing requires a very long time, and the surface quality is still not better than the grinded substrate, which is polished for just 10 min. In this section, both the as-extruded Fe-Cr-Ni alloy substrates were first mechanically grinded and then polished for 5 and 10 min, as shown in Fig. 11. Even though the grinded inner surface (Fig. 11a) looks shiny compared to the as-extruded substrate (Fig. 8c), grooves and scratches induced by the grinding process significantly damaged the surface quality (Fig. 11a′). After IEP for 5 min, grooves and scratches caused by the grinding process are dissolved entirely, and mirror-like reflecting surfaces are obtained, as shown in Figs. 11b, 11b′. Polishing up to 10 min further improved the surface quality (Fig. 11c), and grain boundaries became more evident, as shown in Fig. 11c′.

The WLI morphologies, line profiles, and Ra roughness of the inner surface of grinded Fe-Cr-Ni alloy substrates are given in Fig. 12. As obvious from Figs. 12a, 12b, the WLI morphologies show no significant signs of protrusion, and the initial Sa roughness of grinded substrate (805 nm) has been reduced to 80 nm after IEP for 10 min, which is nearly 90% of the initial value. The line profile and the Ra roughness measured by the profilometer over 15 mm are shown in Fig. 12c. The initial Ra roughness of the grinded substrate was reduced by ∼50% and ∼62% after IEP for 5 and 10 min, respectively. Besides, the line profiles of the polished substrates became relatively very smooth compared to the grinded substrate. Accelerated reduction in the Ra roughness and smoothing of extremely rough line profiles of the grinded Fe-Cr-Ni alloy substrate after a short duration of IEP shows that IEP can efficiently transform a highly rough internal surface into a mirror-like surface, given that poor manufacturing does not seriously deteriorate the initial quality of the substrate.

Conclusions

In this work, the IEP of a Fe-Cr-Ni alloy cylinder produced by extrusion is conducted to improve the inaccessible inner surface. The IEP is conducted in 20 ml H_2SO_4 electrolyte and systematically investigates the effects of cathode diameter and current density on the planarization and current efficiencies, MRR, and surface morphologies of the IEP of grinded Fe-Cr-Ni alloy. Besides, the IEP of the as-extruded inner surface is investigated as a function of

the polishing duration. Finally, the as-extruded and grinded Fe-Cr-Ni substrates are polished simultaneously to investigate surface uniformity, planarization efficiency, and current efficiencies.

Following are the primary conclusions from the study:

1. The electric field simulation predicted maximum current density at protruding regions. And so, the thin passivation layer is highly likely to break at protrusions, and protrudes are more likely to dissolve via isotropic etching holes formation and merging during IEP.
2. The planarization and current efficiencies were found independent of cathode diameter at constant current but improved with growing current density, which is positively related to the passivation layer breakdown, enhanced metal dissolution, and more efficient IEP.
3. Based on the applied current, the IEP process is divided into four stages: (i) electrode passivation, (ii) isotropic etching with passivation layer breakdown under appropriate conditions, (iii) holes merging and new surface unfolding, and (iv) polishing with growing hole diameter.
4. The IEP of the as-extruded Fe-Cr-Ni alloy improved the initial Sa roughness of the functional inner surface by 94% within 46 min, while the highly rough initial condition of the substrate and instantaneously falling off metal lumps seriously influenced the final surface quality and polishing duration.
5. The IEP of the grinded substrate produced a mirror-like surface with substantially improved surface hardness and morphology and realized 37% higher planarization efficiency when as-extruded and grinded Fe-Cr-Ni alloy substrates were simultaneously polished. Poor morphology, low planarization efficiency, and 8% more current efficiency in the case of the as-extruded substrate are because of the falling off the metal lump.
6. The IEP rapidly improved the line profiles and Ra roughness of the grinded substrate. In addition, wall thickness of the as-extruded Fe-Cr-Ni substrates after IEP for 46 min was reduced by 25% compared to the 6% when processed by grinding and subsequent IEP for 10 min.

Acknowledgments

This project is supported by the national natural science foundation of China (52075332, 52035009, 52005243) and the science and technology innovation committee of Shenzhen municipality (JCYJ20200109141003910, KQTD20170810110250357). The authors acknowledge the assistance of SUSTech Core Research Facilities.

ORCID

Muhammad Ajmal Khan https://orcid.org/0000-0001-8255-4995
Hui Deng https://orcid.org/0000-0002-7116-7188

References

1. X. Zhao, W. Song, Z. Yang, J. Liang, and W. Li, *High Strength and Super-High Strength Stainless Steels* (Metallurgical Industry Press, Beijing) (2008).
2. Z. Li, R. Zhang, Q. Zha, Y. Wang, J. Qiang, and C. Dong, "Composition design of superhigh strength maraging stainless steels using a cluster model." *Prog. Nat. Sci: Mater. Int.*, **24**, 35 (2014).
3. L. J. Matienzo, K. J. Holub, and W. Vandatta, "An investigation on surface defects produced during the extrusion of some aluminum alloys." *Appl. Surf. Sci.*, **15**, 307 (1983).
4. J. Han, W. Zheng, and G. Wang, "Investigation of influence factors on surface roughness of micro-scale features." *Precis. Eng.*, **56**, 524 (2019).
5. N. Park, Y. Song, S.-H. Jung, J. Song, J. Lee, H. Lee, H.-M. Sung, and G. Bae, "Numerical and experimental investigation on the surface defect generation during the hot extrusion of Al6063 alloy." *Mater.*, **14**, 6768 (2021).
6. N. Ramachandran, S. Pande, and N. Ramakrishnan, "The role of deburring in manufacturing: a state-of-the-art survey." *J. Mater. Process. Technol.*, **44**, 1 (1994).
7. F. Hashimoto, H. Yamaguchi, P. Krajnik, K. Wegener, R. Chaudhari, H.-W. Hoffmeister, and F. Kuster, "Abrasive fine-finishing technology." *CIRP Ann.*, **65**, 597 (2016).
8. J. Zhao, Y. Xiang, and C. Fan, "A new method for polishing the inner wall of a circular tube with a soft abrasive rotating jet." *Powder Technol.*, **398**, 117068 (2021) .
9. A. P. Nagalingam, H. K. Yuvaraj, V. Santhanam, and S. Yeo, "Multiphase hydrodynamic flow finishing for surface integrity enhancement of additive manufactured internal channels." *J. Mater. Process. Technol.*, **283**, 116692 (2020).
10. C. Cheung, C. Wang, Z. Cao, L. Ho, and M. Liu, "Development of a multi-jet polishing process for inner surface finishing." *Precis. Eng.*, **52**, 112 (2018).
11. F. E. Pfefferkorn, N. A. Duffie, X. Li, M. Vadali, and C. Ma, "Improving surface finish in pulsed laser micro polishing using thermocapillary flow." *CIRP Ann.*, **62**, 203 (2013).
12. A. Okada, Y. Uno, J. McGeough, K. Fujiwara, K. Doi, K. Uemura, and S. Sano, "Surface finishing of stainless steels for orthopedic surgical tools by large-area electron beam irradiation." *CIRP Ann.*, **57**, 223 (2008).
13. Y. Tian, W. S. Gora, A. P. Cabo, L. L. Parimi, D. P. Hand, S. Tammas-Williams, and P. B. Prangnell, "Material interactions in laser polishing powder bed additive manufactured Ti6Al4V components." *Addit. Manuf.*, **20**, 11 (2018).
14. P. Tyagi, T. Goulet, C. Riso, R. Stephenson, N. Chuenprateep, J. Schlitzer, C. Benton, and F. Garcia-Moreno, "Reducing the roughness of internal surface of an additive manufacturing produced 316 steel component by chempolishing and electropolishing." *Addit. Manuf.*, **25**, 32 (2019).
15. U. Ali, H. Fayazfar, F. Ahmed, and E. Toyserkani, "Internal surface roughness enhancement of parts made by laser powder-bed fusion additive manufacturing." *Vacuum*, **177**, 109314 (2020).
16. J. Mingear, B. Zhang, and D. Hartl, "and A. Effect of process parameters and electropolishing on the surface roughness of interior channels in additively manufactured nickel-titanium shape memory alloy actuators." *Addit. Manuf.*, **139**, 1 (2019).
17. W. Han and F. Fang, "Fundamental aspects and recent developments in electropolishing." *Int. J. Mach. Tools Manuf*, **139**, 1 (2019).
18. R. Yi, Y. Zhang, X. Zhang, F. Fang, and H. Deng, "A generic approach of polishing metals via isotropic electrochemical etching." *Int. J. Mach. Tools Manuf*, **150**, 103517 (2020).
19. K. M. Ajmal, R. Yi, Z. Zhan, J. Ji, L. Zhang, and H. Deng, "A novel finishing approach for 3D printed inconel 718 by utilizing isotropic electrochemical etching." *J. Mater. Process. Technol.*, **299**, 117356 (2021).
20. K. M. Ajmal, R. Yi, Z. Zhan, J. Ji, X. Zhang, and H. Deng, "Highly efficient smoothing of Inconel 718 via electrochemical-based isotropic etching polishing." *Precis. Eng.*, **71**, 119 (2021).
21. F. Fang, "Atomic and close-to-atomic scale manufacturing: perspectives and measures." *Int. J. Extrem. Manuf.*, **2**, 030201 (2020).
22. M. Sedlaček, P. Gregorčič, and B. Podgornik, "Use of the roughness parameters S_{sk} and S_{ku} to control friction—a method for designing surface texturing." *Tribol. Trans.*, **60**, 260 (2017).
23. W. Harun, N. Manam, M. Kamariah, S. Sharif, A. Zulkifly, I. Ahmad, and H. Miura, "A review of powdered additive manufacturing techniques for Ti-6Al-4V biomedical applications." *Powder Technol.*, **331**, 74 (2018).
24. R. Konecná, L. Kunz, G. Nicoletto, and A. Baca, "Fatigue crack growth behavior of Inconel 718 produced by selective laser melting." *Frattura. Integr Strutt.*, **10**, 31 (2016).
25. E. Blasco-Tamarit, A. Igual-Muñoz, J. G. Antón, and D. García-García, "Effect of temperature on the corrosion resistance and pitting behaviour of Alloy 31 in LiBr solutions." *Corros. Sci.*, **50**, 1848 (2008).
26. B. K. Nandi and S. Patel, "Effects of operational parameters on the removal of brilliant green dye from aqueous solutions by electrocoagulation." *Arab. J. Chem.*, **10**, S2961 (2017).
27. D. Wang, Z. Zhu, B. He, Y. Ge, and D. Zhu, "Effect of the breakdown time of a passive film on the electrochemical machining of rotating cylindrical electrode in $NaNO_3$ solution." *J. Mater. Process. Technol.*, **239**, 251 (2017).
28. E. S. Lee, "Machining characteristics of the electropolishing of stainless steel (STS316L)." *Int. J. Adv. Manuf. Technol.*, **16**, 591 (2000).
29. D. Wang, Z. Zhu, N. Wang, D. Zhu, and H. Wang, "Investigation of the electrochemical dissolution behavior of Inconel 718 and 304 stainless steel at low current density in $NaNO_3$ solution." *Electrochim. Acta*, **156**, 301 (2015).
30. M. Datta and D. Landolt, "On the role of mass transport in high rate dissolution of iron and nickel in ECM electrolytes—I. Chloride solutions." *Electrochim. Acta*, **25**, 1255 (1980).
31. H. Xin, Y. Shi, L. Ning, and T. Zhao, "Residual stress and affected layer in disc milling of titanium alloy." *Mater Manuf Process.*, **31**, 1645 (2016).
32. T. Hryniewicz, K. Rokosz, J. Valíček, and R. Rokicki, "Effect of magnetoelectropolishing on nanohardness and Young's modulus of titanium biomaterial." *Mater. Lett.*, **83**, 69 (2012).
33. Y. Xia, M. Bigerelle, J. Marteau, P. E. Mazeran, S. Bouvier, and A. Iost, "Effect of surface roughness in the determination of the mechanical properties of material using nanoindentation test." *Scanning Microsc.*, **36**, 134 (2014).
34. D. Greitemeier, C. Dalle Donne, F. Syassen, J. Eufinger, and T. Melz, "Effect of surface roughness on fatigue performance of additive manufactured Ti–6Al–4V." *Mater. Sci. Technol.*, **32**, 629 (2016).